Defects and magnetic properties in Mn-implanted 3C-SiC epilayer on Si(100): Experiments and first-principles calculations

K. Bouziane,* M. Mamor, and M. Elzain
Department of Physics, College of Science, Sultan Qaboos University, P.O. Box 36, Al-Khodh 123, Sultanate of Oman

Ph. Djemia and S. M. Chérif
LPMTM (CNRS-UPR 9001), Université Paris 13, 99 Avenue J.B. Clément, 93430 Villetaneuse, France

(Received 11 June 2008; published 5 November 2008)

The effect of structural and chemical disorder on magnetism of Mn-implanted 3C-SiC epilayer on Si(100) is investigated experimentally using Rutherford backscattering channeling spectroscopy (RBS/C), x-ray diffraction (XRD), micro-Raman spectroscopy (μRS), and magnetometry, and theoretically using *ab initio* calculations. A single 3C-SiC epilayer on Si(001) was implanted at room temperature (RT) with Mn ions at 80 keV and at a dose of 5×10^{15} cm^{-2}. RBS data show the formation of a highly disordered implanted layer of $\sim$45 nm with a peak Mn atomic concentration of $\sim$1.8% randomly distributed, in agreement with the stopping and range of ions in matter (SRIM) simulation. The experimental results of magnetic moment per Mn are interpreted by assuming that the implanted layer consists of two respective main regions, C–rich and Si–rich regions, as reflected by the presence of a graphitic phase, in which the local atomic environment of Mn is essentially C. Annealing seems to favor Mn substitution into Si sites, indicated by the substantial expansion of the lattice constant due to larger covalent Mn radius as observed by XRD and due to a high local tensile strain determined from μRS. This interpretation is also supported by recent calculations, showing that it is energetically favorable for Mn to substitute Si sites. The temperature dependence of magnetization shows an insulatinglike character for the as-implanted film and metalliclike for the annealed-implanted film with Curie temperature above RT. In addition, the magnetic moment per Mn increases strongly with annealing from 0.23 to $0.65\mu_B$. The experimental behavior is supported by our *ab initio* calculations, showing that magnetism in Mn-doped 3C-SiC can be enhanced by carefully growing a structure with Mn in Si sites using a C-deficient SiC host, possibly resulting in localized magnetic interactions.

DOI: 10.1103/PhysRevB.78.195305 PACS number(s): 75.50.Pp, 71.15.Mb

I. INTRODUCTION

Recently, dilute magnetic semiconductors (DMSs), where a host semiconductor is doped with magnetic impurity (transition-metal or rare-earth element), have been extensively studied. In particular, ferromagnetism in the vicinity of room temperature (RT) was achieved in Mn-implanted Si single crystal wafers.[1,2] The host Si presents, however, some limitations for obtaining DMSs with high Curie temperature (T_C). This is because its band gap (1.2 eV) is relatively very small and lower T_C is expected.[3] Moreover, the hardness of Si is small and the implantation process can cause severe damage to the material. An alternative host material is SiC. Indeed, SiC is structurally similar to Si except that half of the Si atoms are replaced by C atoms in tetrahedral symmetry. SiC is also compatible with the very mature silicon technology. Considering the potential of SiC for high-power and high-temperature electronics, Mn-doped SiC might be an excellent candidate for spintronics applications (e.g., utilizing the electron's spin degree of freedom in addition to its charge) with possibly high T_C. This is due to its wide band gap of $\sim$2.4 eV at 300 K,[4] excellent transport properties, dopability, and hardness. Due to lattice mismatch (20%) and thermal mismatch (8%),[5,6] heteroepitaxy of SiC on silicon substrate always results in growth of 3C-SiC with a very high density of crystallographic structural defects such as stacking faults, microtwins, and inversion domain boundaries. In general, this results in native *n*-type doping.

Recently, Mn-implanted *n*-type 3C-SiC, by ion implantation at a fluence of 1×10^{16} cm^{-2} and implantation energy of 350 keV (Ref. 7) and similarly in Mn-implanted 6H-SiC,[8] were found to exhibit ferromagnetism below 245 K. In the latter studies, the enhancement of magnetism of Mn-implanted SiC after annealing was attributed to lattice relaxation. The annealing experiments show that the ferromagnetism of Mn-implanted SiC is the result of a delicate interplay between long-range carrier-mediated interaction between Mn ions and local effects mainly driven by the presence of intrinsic or implantation-induced defects. It has been theoretically predicted that when relaxation is included, the Mn interacting neighboring pairs in Mn-doped 3C-SiC prefer a ferromagnetic alignment, which is also in agreement with Anderson-Hasegawa model (because the bands are not half filled).[9,10] In the latter study,[9] it is shown that the magnetic moment per Mn is of the order of $1\mu_B$ regardless of the Mn substitutional site (Si or C) per unit cell of 3C-SiC. In contrast, Shaposhnikov and Sobolev[11] have shown using *ab initio* calculations that 3C-SiC with Mn at either Si site (Mn_{Si}) or C site (Mn_C) is a half-metallic ferromagnetic system but with different magnetic moments for Mn_{Si} and Mn_C, irrespective of Mn atomic concentration below 16%.

It is generally accepted that ferromagnetism in DMSs is a carrier-mediated mechanism, and therefore, structural and chemical defects should play a central role in the electronic transport. In this work, we assess the structural and chemical disorders in the Mn-implanted single-crystal 3C-SiC epilayer

 ©2008 The American Physical Society

before and after annealing by using x-ray diffraction (XRD), Rutherford backscattering spectroscopy (RBS) in both random and channeling (RBS/C) modes, and micro-Raman spectroscopy (μRS). The magnetic properties are investigated by using magnetometry [vibrating sample magnetometer (VSM)]. An attempt is made to correlate the defects and magnetic properties of the Mn-implanted SiC film on the light of the full-potential linear-augmented plane waves (FP-LAPW) method, which utilizes the generalized gradient approximation (GGA).[12,13] In this work we show that the enhancement of magnetism of Mn-implanted 3C-SiC due to annealing can be attributed to the Mn_{Si} and its vacancy environment.

II. TECHNIQUES

The epitaxial of a micrometric single 3C-SiC film on Si(100) substrate has been performed in the Microfabrication Laboratory at Case Western Reserve University using an atmospheric pressure chemical vapor deposition system. The conditions of deposition can be found elsewhere.[14] The 3C-SiC epilayer is *n*-type doped due to native defects. RT Mn implantation was performed at The Ion and Molecular Beam Laboratorium (IMBL) in Leuven (Belgium) with a dose of 5×10^{15} Mn/cm^2 at an energy of 80 keV. The structure was investigated at room temperature using powder x-ray diffraction with a Philips PW 1700 diffractometer with Cu Kα radiation. Micro-Raman experiments were conducted in the backscattering geometry along the [100] axis with a Labram high-resolution spectrometer and a $\times100$ objective. A blue light irradiation of wavelength 488 nm and an average of ten accumulations and duration of 5 s were used with a 30-mW incident power. Crystalline quality and defects introduced in the implanted SiC layers were characterized by RBS/C using a 1.57-MeV He^+ beam and a scattering angle of 105° since this is a nondestructive technique which allows depth determination of the distribution of ions and defects present in the film. The magnetization measurements were carried out by using a VSM with a sensitivity better than 1.0×10^{-6} emu in a magnetic field up to 13.5 kOe and at temperatures down to 77 K. The VSM was calibrated using pure nickel (Ms $=54.9$ emu/g). The diamagnetic contribution from the sample holder was obtained from independent M-H loops and the diamagnetic signal from the sample holder; the signal of both nonimplanted SiC and Si substrate were subtracted from the film's data. The uncertainty in measuring the absolute value of magnetization for the films is about 5%.

We have used the FP-LAPW method as employed in the WIEN2K code, where various forms of V_{xc} are available.[12,13] In the calculation presented here we have used the GGA of Perdew-Burke-Ernzerhof. The conventional fcc unit cell is used as a primitive unit cell to study the electronic structure of Mn impurities in the host cubic SiC with and without vacancies. An angular momentum cutoff of $l_{max}=10$ and atomic spheres of radii $R_{MT}=1.77$ au were used. The augmented plane-wave local orbitals (APW+lo) bases were used for all valence states. These improve the results for local orbitals inside the muffin-tin radius. The wave functions in the interstitial region were expanded in plane waves with a cutting off of $K_{max}=7/R_{MT}$, while the electron density was Fourier expanded up to $G_{max}=14$. A mesh of 343 special k points was taken for the irreducible Brillouin-zone wedge.

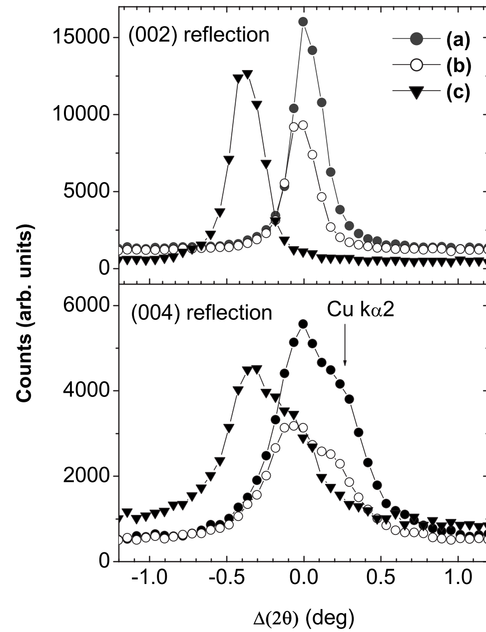

FIG. 1. X-ray diffraction patterns of the (a) virgin 3C-SiC, (b) as-implanted Mn/3C-SiC, and (c) annealed Mn/3C-SiC films recorded at room temperature. The angular positions of (002) and (004) reflections of the virgin are taken as a reference.

III. RESULTS AND DISCUSSION

Figure 1 shows the XRD patterns for the (002) and (004) reflections of the virgin 3C-SiC, as-implanted and annealed Mn-doped 3C-SiC films. The shoulder observed at high angle of the Bragg peaks is related to Cu Kα_2 radiation. The position of the Si(004) substrate ($2\theta=69.7°$) was the same for all samples. The angular positions of (002) and (004) reflections of the virgin were taken as a reference. While the positions of (002) or (004) peaks of the as-implanted film slightly shift to lower angle [$\Delta a_\perp/a=(a-a_0)/a_0\cong0.9\times10^{-3}$, a_0 and a being the lattice constants of the virgin and implanted film, respectively] as compared to that of the virgin sample, a relatively larger shift ($\Delta a_\perp/a\cong8.5\times10^{-3}$) is observed for the annealed sample. This induced strain may be an indication of the incorporation of a partial amount of implanted Mn in the SiC lattice due to the larger Mn covalent radius.[9] Implantation-induced defects such as vacancies and interstitials can also cause strain, which can be another origin of the observed shifts. From the XRD patterns, reflections related to Mn compounds such as Mn silicides[15,16] or Mn carbides have not been observed.

In order to check the implantation-induced damage and the lattice location of Mn, the samples were analyzed by RBS in random and channeling modes. Figure 2 shows the RBS spectra for the virgin and as-implanted samples. The degree of lattice disordering (χ_{min}) (Ref. 17) for Si signal in the virgin film is ~2%, and it is above 80% for the as-

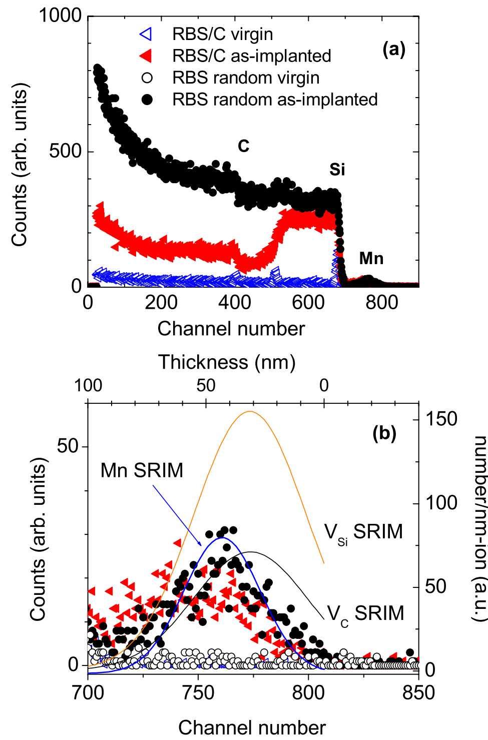

FIG. 2. (Color online) (a) RBS random and channeling along SiC[001]. Random (○) and channeling (◁) for the virgin SiC sample. Random (●) and channeling (◀) for the as-implanted Mn-SiC, (b) Mn signals (data point). No Mn channeling was observed either for as-implanted or annealed samples, SRIM simulations (solid lines) of 3C-SiC implanted with Mn at energy of 80 keV for Mn profile, and Si (V_{Si}) and C (V_C) vacancies. The random RBS for annealed-implanted sample is similar to that of the as-implanted and it is not shown here for clarity. It is to be noted that the Si random signals for the virgin (○) and as-implanted (●) samples are the same.

implanted one. This reflects the good crystalline quality of the virgin and highly disordered implanted layer due to high concentration of defects. For the Mn signal [Fig. 2(b)] χ_{min} is about 100%, indicating a random distribution of Mn. The RBS signal of Mn for the annealed sample displays identical Gaussian distribution centered around the projected range $Rp \sim 45$ nm. The Rutherford Universal Manipulation Program (RUMP) (Ref. 18) simulation of the RBS spectrum for the as-implanted sample gives a concentration of Mn of ~1.8% in very good agreement with our SRIM simulations[19] considering the implanted dose of 5×10^{15} cm^{-2} [Fig. 2(b)]. In order to get more insights about the implantation-induced defects, we have carried out SRIM simulations. The profile results for C vacancy and Si vacancy are shown in Fig. 2(b). The profiles have Gaussian shapes with a peak concentration of either C or Si vacancies centered at ~30 nm, the number of Si vacancies being double C vacancies [Fig. 2(b)]. Due to the strong chemical bonding in the 3C-SiC compound and, hence, reduced mobility of implantation-induced defects, a number of permanent defects subsist in the implanted sample after annealing as deduced from RBS results and inferred from μRS analysis discussed below.

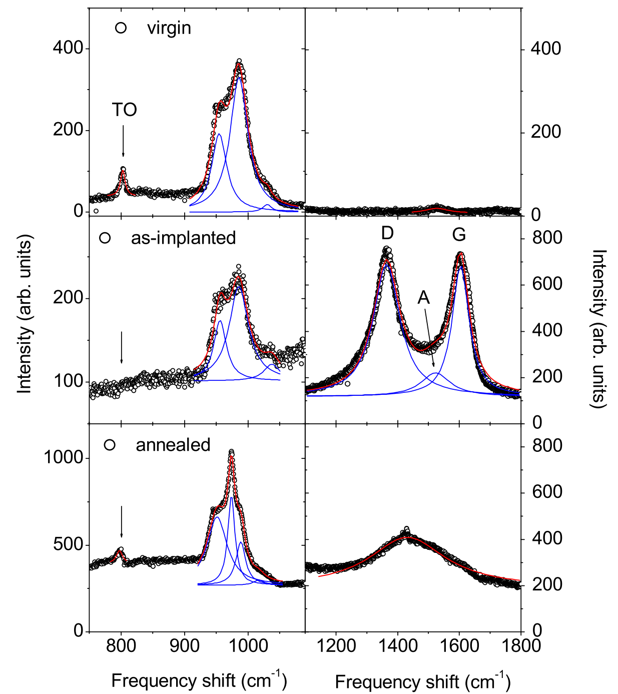

FIG. 3. (Color online) Micro-Raman (wavelength 488 nm) spectra of the virgin 3C-SiC, as-implanted and post-annealed films. The left panel is the corresponding C-C features. The solid lines are Lorentzian fits.

Inspection of the diffusion process due to annealing has been analyzed from the relative positions of the surface RBS signal of Si and RBS Mn peak, as well as their relative intensity. The relative channel peak position of Mn relative to Si surface remains the same after annealing (not shown in Fig. 2 for clarity). The relative Mn to Si RBS intensity does not change with annealing, too. These results suggest that Mn (in combination with the analysis of μRS results below) has been redistributed locally within the implanted layer after annealing.

The micro-Raman spectra for the three samples (virgin, as-implanted, and annealed) are shown in Fig. 3. The ionic character of 3C-SiC causes the splitting of the doubly-degenerated TO(Γ) mode and LO(Γ) mode at the $\Gamma(q=0)$ point in μRS.[20] Although the TO mode is forbidden in the backscattering geometry for the zinc-blende structure, it is observed in the virgin sample due to the imperfection of the 3C-SiC film surface and to the nearlike backscattering geometry in microscope. While the TO mode is present for the virgin (~795 cm^{-1}) and annealed (~793 cm^{-1}) samples, it is totally suppressed for the as-implanted sample due to the highly disordered implanted layer. The line shape of the SiC-related LO mode was well fitted using three Lorentzians (M_1-M_3) for the virgin and as-implanted samples corresponding to M_1 (~947 cm^{-1}) possibly due to a feature associated with the modifications at the interface between the 3C-SiC epilayer and Si substrate,[21,22] M_2 mode associated with LO of 3C-SiC (~978 cm^{-1}), and a third M_3 mode similarly reported in Ref. 23 but not identified. Four Lorentzians (M_1-M_4) were, however, required to fit the LO-related

TABLE I. Position of the Raman peaks (wavelength 488 nm) observed in the virgin single-crystal 3C-SiC, as-implanted and annealed-implanted Mn-SiC films. See text for the definition of M_1-M_4 modes. G and D are the graphitic and disordered graphitic phase modes, and the A is the amorphous graphitic mode. All modes are expressed in cm^{-1}.

	Si-C region					C–C region		
Sample	TO(Γ)	M_1	M_2	M_4	M_3	D	A	G
Virgin	794.8	946.6	977.8		1022.4		1518.9	
As-implanted		948.0	977.6		1029.7	1356.3	1515.3	1596.1
Annealed	792.6	947.8	969.0	983.4	1013.5		1426.2	

modes for the annealed-implanted sample. The LO mode (M_2) of 3C-SiC is about 969 cm^{-1} for the annealed sample, suggesting that the film is under tensile strain,[24] in agreement with XRD results. The additional feature (M_4) at $\sim$983 cm^{-1} can be attributed to the coupled plasmon LO-phonon mode (CPLOM).[25] The results of the fitting are displayed in Table I.

It should be pointed out that the intensity of the feature around the LO mode of the as-implanted sample is substantially diminished relative to the virgin sample due to the disordering. A strong feature (Fig. 3, left panel) is observed in the high-frequency C-C range, due to Mn implantation, which was fitted using three Lorentzians associated with the two bands G (graphitic phase: $\sim$1596 cm^{-1}) and D (disordered graphitic phase: $\sim$1356 cm^{-1}), and a broader feature centered at about 1515 cm^{-1} assigned to amorphous graphitic phase A.[26] This graphitic phase does not produce any characteristic peak in the XRD pattern. The μRS analysis shows that implantation has induced a high degree of disorder, consisting principally of sp^2 carbon bonds.[27] A partial recovery of the crystallinity after annealing is reflected by the reduction in intensity of the graphitic phase features and enhancement of the LO-related features of 3C-SiC. This suggests that a certain mutual interdiffusion of C and Si took place during the annealing treatment.

Considering the above experimental and SRIM simulation results—(i) strain and microstrain observed by XRD and μRS, respectively, (ii) random distribution of Mn and its local redistribution after annealing as deduced from RBS and μRS, (iii) partial recovery of crystallinity determined by μRS, and (iv) taking into account V_{Si} and V_C distribution from SRIM simulations—we can reasonably assume the existence of various zones, respectively rich in C (surface of the SiC epilayer) and in Si in the presence of various types of defects, particularly V_C and V_{Si}.

Magnetization curves $M(H)$ at RT for the as-implanted and annealed films are shown in Fig. 4 (bottom). The linear diamagnetic signal background of both virgin SiC/Si and sample holder was subtracted for the displayed data. The virgin SiC shows pure diamagnetic signal. The magnetic moment per Mn at RT is found to increase from $0.23\mu_B$ for the as-implanted to $0.65\mu_B$ for the annealed film (a relative change of $\sim$180%). The coercive field remained constant at a value of 100 Oe for both as-implanted and annealed films. The normalized temperature-dependent magnetization curve $[M/M(77\ K)$ vs T, $M(77\ K)$ being the magnetization of each sample at 77 K$]$ of the implanted sample before and after annealing, measured under 2 kOe, is shown in Fig. 4 (top). The $M(T)$ curve is nearly concave for the as-implanted sample in the range 77–300 K. The $M(T)$ curve for the annealed sampled could be fitted with the Bloch's $T^{3/2}$ law in the same temperature range (77–300 K) but a better fit was obtained by considering a linear variation in M vs T, with Curie temperature above RT. Considering the ferromagnetic M-H loops (Fig. 4), the $M(T)$ behavior for both samples is therefore in contrast to the Brillouin-type behavior predicted by the mean field theory of Weiss and Stoner.[28] Such concave and linear behaviors of $M(T)$ were usually attributed to insulating and metallic characters, respectively, in DMS systems.[29]

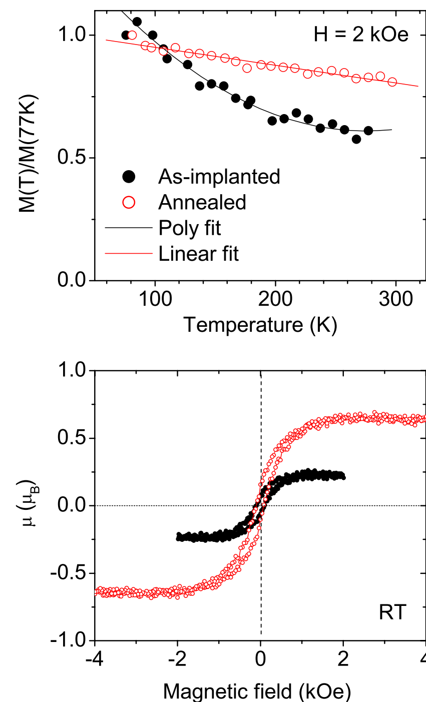

FIG. 4. (Color online) (Bottom) Ferromagnetic hysteresis loops at room temperature for as-implanted (black) and annealed (red) Mn-SiC films. The linear background diamagnetic signal of virgin SiC/Si was subtracted for displayed data. (top) Temperature dependence of the normalized magnetization for the as-implanted (black) and annealed-implanted (red) samples, with $M(77\ K)$ being the magnetization of each sample at 77 K.

TABLE II. Magnetic moment (μ_B) per Mn atom in Mn-doped 3C-SiC for different substitution and vacancy types obtained from FP-LAPW utilizing the GGA in WIEN2K scheme.

	Mn_{Si} No V	Mn_C No V	Mn_{Si} V_{Si}	Mn_{Si} V_C	Mn_C V_{Si}	Mn_C V_C
Magnetic moment (μ_B)	2.30	0	~1.00	2.57	0.88	0
Configuration	I	II	III	IV	V	VI

In an attempt to shed more light on the metalliclike $M(T)$ behavior and enhancement of the magnetic moment of the annealed-implanted sample, we have performed *ab initio* calculation on Mn impurities in SiC with and without Si and C vacancies.

We focus our *ab initio* calculations on the possible role played by V_{Si} or V_C in the enhancement of magnetism of Mn implanted due to annealing. In fact, the irradiation-induced monovacancies at Si (V_{Si}) and carbon (V_C) sublattice sites have been experimentally observed[30,31] and theoretically demonstrated.[32] Generally, V_{Si} or V_C were found to be stable at room temperature and have high spin $S=3/2$ and low spin $S=1/2$, respectively. We have performed our calculations by considering Mn at Si sites (Mn_{Si}) or at C sites (Mn_C), as well as different configurations of defects. The corresponding results are displayed in Table II. Typical densities of states (DOSs) corresponding to configurations IV and V (see Table II) are shown in Fig. 5. Examination of this figure provides evidence of a strong shift between DOS-up and DOS-down for $Mn_{Si}+V_C$ (labeled $SiC_V:Mn_{Si}$) configuration (IV), indicating the presence of a large local magnetic moment of $2.57\mu_B$ on the transition-metal atoms. The later system is also nearly half metallic. For Mn_C+V_{Si} ($Si_VC:Mn_C$) configuration (V), the relative change between up and down DOSs is not very significant, leading to a small moment on Mn of $0.88\mu_B$.

For $SiC:Mn_{Si}$, Si vacancy yields to a remarkable decrease in the magnetic moment μ ($2.30\rightarrow1.00\mu_B$), while the C vacancy ($SiC_V:Mn_{Si}$) contributes to a noticeable enhancement of μ ($2.30\rightarrow2.57\mu_B$). For $SiC:Mn_C$, the situation is almost

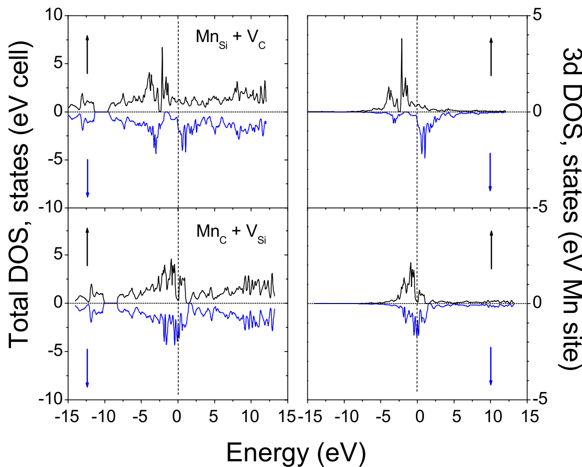

FIG. 5. (Color online) Typical total DOS (left panel) and the corresponding three-dimensional Mn DOS (right panel) of Mn-doped 3C-SiC for (top) Mn substituted at Si (Mn_{Si}) with C vacancy (V_C) with $\mu=2.57\mu_B$, and (bottom) Mn_C and V_{Si} with $\mu=0.88\mu_B$.

reversed in the sense that μ is increased ($0\rightarrow0.88\mu_B$) for Si vacancy and μ remains zero for C vacancy.

It should be stressed that secondary magnetic phases, such as Mn silicides or Mn carbides, were not detected by the different techniques used in this work. Although the eventual presence of such phases cannot be ruled out totally, we have, however, some good reasons to exclude them. First, the manganese was recently theoretically shown not to be a good carbide former.[9] Second, the secondary magnetic phases, if they exist and are stable, should grow with annealing, and therefore, magnetic parameters such as coercivity H_c are expected to change. This is not the case for our film since H_c remains constant (~100 Oe) with annealing.

It is well established that the electrical activity of magnetic impurities such as Mn in DMSs is partial so that the total number of carriers introduced by Mn is less than the concentration of Mn itself.[29] The magnetism is believed to be mediated by carriers and, hence, is strongly affected by their concentration. In order to make an adequate comparison between the experimental and theoretical magnetic moments, it is therefore more appropriate to consider the ratio of magnetic moments. This approach is correct in the sense that the effective region of where Mn atoms exist is similar before and after annealing; only redistribution of Mn due to annealing was observed as discussed above. By a careful inspection of Table II, the experimental magnetic moments ratio $[\mu_{\text{as-implanted}}/\mu_{\text{annealed}}=0.23/0.65=0.35]$ was found to correspond to the ratio of the magnetic moments of configuration V to IV: $\mu_V/\mu_{IV}=0.88/2.57=0.34$ using our FP-LAPW calculations. This is consistent with the picture that Mn exists mainly in the C-rich region in the SiC matrix, and annealing would favor Mn to substitute Si from thermodynamic considerations.[9] This result suggests that the Mn-substitution site and vacancy type are crucial in determining the largest magnetic moment with the highest Curie temperature T_C.

The fact that both LO and TO modes of the annealed sample experience a down-frequency shift relative to that of the virgin indicates the presence of tensile microstrain in the annealed film.[24] The strain and change in force constants usually cause an almost equal shift for the TO and LO mode frequencies. The LO-TO splitting decreases from the virgin (ω_{LO}-$\omega_{TO}=183$ cm^{-1}) to the annealed-implanted sample (176.4 cm^{-1}). Hence, this reduction in the LO-TO splitting would not be due to stress, but in combination of the redshift of the LO and TO modes that are generally attributed to a change of the polarization field due to defects. The relative change of the effective charge Q ($Q\propto\sqrt{\omega_{LO}^2-\omega_{TO}^2}$) on ions was estimated from μRS considering that the dc dielectric constant ε_0 does not vary significantly.[33] We found that the relative change of Q between the virgin and annealed-implanted film is relatively small ($\Delta Q/Q\cong2.3\%$), and

hence, the effective charge on ions remained nearly the same, regardless of the Mn implantation and annealing process. The presence, however, of the CPLOM in μRS spectrum of the annealed sample may result from the reduction of carriers' concentration, in which case defects act as traps for electrons for such *n*-type Mn-doped 3C-SiC. This may suggest that the magnetic interactions are localized in this system.

It should be noted that more accurate calculations should consider interstitials, extended defects, and possibly defect complexes, in addition to C or Si vacancies. It is peculiar to determine experimentally the extended and complex defects and, hence, their effects on magnetism. While the presence of vacancies implies the presence of interstitials, the consideration of both vacancies and interstitials in the calculations would result in a complex situation such as several relative positions of interstitial with respect to vacancies and Mn. Our task was to find out the correlation between the vacancies (V_{Si} or V_C) evidenced experimentally in this work and magnetism in the Mn-implanted 3C-SiC epilayer. The role of other defects may be the subject of a future work.

IV. CONCLUSION

In summary, Mn implantation at RT with energy 80 keV at a dose of 5×10^{15} cm^{-2} into the 3C-SiC(001) epilayer introduces a large amount of disorder and crystallinity can be partially recovered by annealing the implanted sample at 750 °C for 2 h. This results in an increase in the magnetic moment per Mn from 0.23 to 0.65μ_B with the Curie temperature above RT. From both experimental and *ab initio* calculation results, it is shown that the substitutional site of Mn and its environment such as Si and C monovacancies play a crucial role on the magnetism in Mn-doped 3C-SiC.

ACKNOWLEDGMENTS

The authors would like to thank Ch. Zorman for providing the single 3C-SiC films. Two of the authors (K.B. and M.M.) are grateful to A. Vantomme from K. U. Leuven for his assitance in Mn implantation and RBS techniques. M. Maaza is also acknowledged for useful comments on RBS data.

*Corresponding author; bouzi@squ.edu.om

[1] M. Bolduc, C. Awo-Affouda, A. Stollenwerk, M. B. Huang, F. G. Ramos, G. Agnello, and V. P. LaBella, Phys. Rev. B **71**, 033302 (2005).
[2] H. W. Wu, C. J. Tsai, and L. J. Chen, Appl. Phys. Lett. **90**, 043121 (2007).
[3] T. Dietl, H. Ohno, F. Matsukura, J. Cibert, and D. Ferrand, Science **287**, 1019 (2000).
[4] J. A. Freitas, Jr., *Properties of Silicon Carbides*, edited by G. L. Harris, EMIS Data Reviews Series, No. 13 (INSPEC, London, 1995, pp. 29–41).
[5] P. Pirouz, C. M. Chorey, and J. A. Powell, Appl. Phys. Lett. **50**, 221 (1987).
[6] P. Pirouz, C. M. Chorey, T. T. Cheng, and J. A. Powell, in *Heteroepitaxy on Silicon II*, MRS Symposia Proceedings No. 91, edited by J. C. Fan, J. M. Phillips, and B.-Y. Tsaur (Materials Research Society, Pittsburgh, PA, 1987), p. 399.
[7] F. Takano, W. Wang, H. Akinaga, H. Ofuchi, Sh. Hishiki, and T. Ohshima, J. Appl. Phys. **101**, 09N510 (2007).
[8] S. J. Pearton, Y. D. Park, C. R. Abernathy, M. E. Overberg, G. T. Thaler, J. Kim, F. Ren, J. M. Zavada, and R. G. Wilson, Thin Solid Films **447-448**, 493 (2004).
[9] M. S. Miao and W. R. L. Lambrecht, Phys. Rev. B **68**, 125204 (2003).
[10] P. W. Anderson and H. Hasegawa, Phys. Rev. **100**, 675 (1955).
[11] V. L. Shaposhnikov and N. A. Sobolev, J. Phys.: Condens. Matter **16**, 1761 (2004).
[12] P. Blaha, K. Schwarz, G. K. H. Madsen, D. Kvasnicka, and J. Luitz, *WIEN2k, An Augmented Plane Wave Plus Local Orbitals Program for Calculating Crystal Properties* (Karlheinz Schwarz, Technical Universitat Wien, Austria, 2001).
[13] S. Cottenier, *Density Functional Theory and the Family of (L)APW-Methods: A Step-by-Step Introduction* (Institute voor Kern-en Stralingsfysica, K. U. Leuven, Belgium, 2002).
[14] Ph. Djemia, Y. Roussigné, G. F. Dirras, and K. M. Jackson, J. Appl. Phys. **95**, 2324 (2004).
[15] Shengqiang Zhou, K. Potzger, Gufei Zhang, A. Mücklich, F. Eichhorn, N. Schell, R. Grötzschel, B. Schmidt, W. Skorupa, M. Helm, J. Fassbender, and D. Geiger, Phys. Rev. B **75**, 085203 (2007).
[16] D. Senk and G. Borchardt, Microchim. Acta **80**, 477 (1983).
[17] The parameter χ_{min} is defined as the ratio of the backscattering yield at RBS channeling condition to that for a random RBS beam incidence.
[18] RUMP (Rutherford Universal Manipulation Program) is a computer code and a FORTRAN program, which performs the disorder analysis from the RBS spectra; L. R. Doolittle, Nucl. Instrum. Methods Phys. Res. B **9**, 344 (1985).
[19] J. F. Ziegler, J. P. Biersack, and U. Littmark, *The Stopping and Range of Ions in Solids Stopping and Ranges of Ions in Matter* (Pergamon, New York, 1984), Vol. 1.
[20] A. Jayaraman, Rev. Mod. Phys. **55**, 65 (1983).
[21] Z. A. Feng, W. J. Choyke, and J. A. Powell,J. Appl. Phys. **64**, 6827 (1988).
[22] L. A. Falkovsky, J. M. Bluet, and J. Camassel, Phys. Rev. B **57**, 11283 (1998).
[23] J. Zhu, S. Liu, and J. Liang, Thin Solid Films **368**, 307 (2000).
[24] S. Rohmfeld, M. Hundhausen, L. Ley, Ch. A. Zorman, and M. Mehregany, J. Appl. Phys. **91**, 1113 (2002).
[25] S. Nakashima, T. Kitamura, T. Mitani, H. Okumura, M. Katsuno, and N. Ohtani, Phys. Rev. B **76**, 245208 (2007).
[26] B. Marcus, L. Fayette, M. Mermoux, L. Abello, and G. Lucazeau, J. Appl. Phys. **76**, 3463 (1994).
[27] T. Jawhari, A. Roig, and J. Cassado, Carbon **33**, 1561 (1995).
[28] T. Kaneyoshi, *Introduction to Surface Magnetism* (CRC, Boca Raton, FL, 1990).
[29] C. Timm, J. Phys.: Condens. Matter **15**, R1865 (2003).
[30] H. Itoh, A. Kawasuso, T. Ohshima, M. Yoshikawa, I. Nashiyama,

S. Tanigawa, S. Misawa, H. Okumura, and S. Yoshida, Phys. Status Solidi A **162**, 173 (1997).

[31] T. Ohshima, A. Uedono, K. Abe, H. Itoh, Y. Aoki, M. Yoshikawa, S. Tanigawa, and I. Nashiyama, Appl. Phys. A: Mater. Sci. Process. **67**, 407 (1998).

[32] A. Zywietz, J. Furthmüller, and F. Bechstedt, Phys. Rev. B **59**, 15166 (1999).

[33] S. Nakashima, T. Mitani, J. Senzaki, H. Okumura, and T. Yamamoto, J. Appl. Phys. **97**, 123507 (2005).